VIII-Ⅱ-1. Project Research

Project 8

PR8 Irradiation Effects on Microstructural Evolution in Materials Irradiated by Particles with High Energy

Q. Xu

Research Reactor Institute, Kyoto University

OBJECTIVES: Maintenance the safety of nuclear reactors is important. Neutron irradiation degrades mechanical properties of materials. Thus the study of nucleation and growth of irradiation defects in materials is significant to predict irradiation effect. Kyoto University research reactor, and other irradiation facilities, such as ions, electrons and γ rays, have also been used in the present project research to clarify the damage structural development.

RESULTS: The allotted research subject (ARS) and the name of co-researches in each ARS are listed below. A number of important data were already obtained. Details are presented in this progress reports.

ARS-1
Persistent photoconductivity in electron-irradiated single crystal ZnO bulk: dual light illumination effect
(K. Kuriyama, T. Oga, T. Ida, K. Kushida, and Q. Xu)

ARS-2
X-ray diffraction analysis of ZnO implanted with Sn^+ at room temperature and 110 K
(G.T. Dang, N. Nitta, M. Taniwaki and T. Yoshiie)

ARS-3
Study on formation and recovery of damage in irradiated crystalline materials
(A. Kinomura, K. Sato, Q. Xu and T. Yoshiie)

ARS-4
Orange emission of calcites by gamma rays
(T. Awata, T. Kishino, F. Maki and Q. Xu)

ARS-5
Annealing behavior of thermal diffusivity and positron annihilation lifetime in 30MeV electron-irradiated ceramics
(M. Akiyoshi, I. Takagi, T. Yoshiie, Q. Xu, K. Sato)

ARS-6
Defects in a Zr-Nb alloy studied by positron annihilation and atom probe tomography
(Y. Nagai, T. Toyama, Y. Matsukawa, Y. Shimizu, A. Kuramoto, H. Takamizawa, Y. Kakubo, K. Inoue, T. Yoshiie, Q. Xu and K. Sato)

ARS-7
Defects study for iron alloys damaged by electron irradiation
(F.Hori, M.Maruhashi, N. Onodera, A.Ishii, S.Mineno, A.Iwase, Q.Xu, K.Sato and T.Yoshiie)

ARS-8
Recovery process of neutron-irradiated vanadium alloys in post-irradiation annealing treatment
(K. Fukumoto, M. Iwasaki and Q. Xu)

ARS-9
Damage evolution in neutron-irradiated metals during neutron irradiation at elevated temperatures
(I.Mukouda, K. Yamakawa, T. Yoshiie, Q. Xu)

ARS-10
Effects of thermal aging and irradiation on mechanical properties of Fe-Cr ferritic alloys
(R. Kasada, Y. Sakamoto, K. Yabuuchi, A. Kimura, K. Sato, Q. Xu, T. Yoshiie)

ARS-11
Radiation resistance of nanocrystalline Ni by neutron irradiation
(H. Tsuchida, A. Itoh, K. Sato, T. Yoshiie, Q. Xu)

ARS-12
Interaction between deuterium and defects in tungsten
(K. Sato, R. Tamiya, Q. Xu and T. Yoshiie)

ARS-13
Irradiation effects on stress loading property of refractory metal at high temperature
(K. Tokunaga, K. Araki, T. Fujiwara, T. Hotta, Q. Xu, T. Yoshiie)

採択課題番号 23P8　材料の組織変化に及ぼす高エネルギー粒子線の照射効果　　プロジェクト

（京大・原子炉）徐　虬

PR8-1 Persistent Photoconductivity In Electron-irradiated Single Crystal ZnO Bulk: Dual Light Illumination Effect

K. Kuriyama, T. Oga, T. Ida, K. Kushida[1] and Q. Xu[2]

College of Engineering and Research Center of Ion Beam Technology, Hosei University
[1]Osaka Kyoiku University
[2]Research Reactor Institute, Kyoto University

INTRODUCTION: Some models of Persistent Photoconductivity (PPC) mechanism have been theoretically proposed [1, 2], indicating that the oxygen vacancies (V_O) with various charge states (V_O^+ or V_O^{2+}) are related to PPC in ZnO. In the present study, in order to study the origin of the PPC, we use the dual light illumination (DLI), namely, the illumination with blue LED and subsequently, the illumination with red or infrared LED.

EXPERIMENT: The ZnO single crystals used in the present study were grown at Tokyo Denpa Co, Ltd. using the hydrothermal method. A 30 MeV electron-irradiation was performed at room temperature, using an electron linear accelerator facility at Kyoto University Research Institute. A beam current and irradiation dose were 18 μA/cm^2 and 5×10^{17} e$^-$/cm^2, respectively.

RESULTS: Fig. 1 shows the decay of PPC under the DLI (first, the illumination with blue LED for 20 min and subsequently, with red or infrared LEDs for 20 min). All these spectra were normalized after subtracting the dark current. The excitation with red and infrared LED showed the remarkable reduction of PPC, suggesting that electrons in the origin of the PPC were excited to higher unoccupied states.

Fig. 2(a) shows PPC spectra measured at various temperatures between 90 and 300 K. To study variations of PPC under the DLI, after turning off the blue LED, the sample was held in the dark for 60 min and subsequently exposed to the infrared LED for 20 min. Both the current reduction in PPC and the slight increase in the photocurrent were observed. The threshold temperature for the increase and decrease in the photocurrent was ~160 K. These results imply that the electrons in the origin of PPC are sensitive to the sample temperature. PPC curves of 250 and 300 K were fitted by the least square method with the stretched exponential function [3], $I(t) = I(0) \exp[-(t/\tau)\beta]$, which was used in our previous study [4], as shown in Fig. 2. The fitting parameters, τ and β values, were 2.4×10^5 s and 0.11 at 250 K and 1.0×10^4 s and 0.27 at 300 K, respectively. The stretched exponential functions were well fitted with the experimental values except for the slight increase in the photocurrent caused by the exposure to the infrared LED. Thus, the slight increase in the photocurrent observed here is not directly related to PPC observed in the present study.

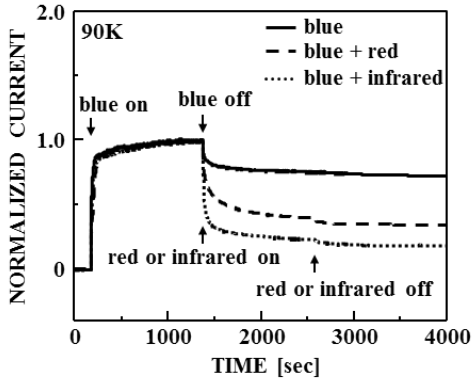

Fig. 1. Persistent Photoconductivity (PPC) measured at 90 K under the dual light illumination (DLI), namely, the illumination with blue LED for 20 min and subsequently, the illumination with red or infrared LED for 20 min.

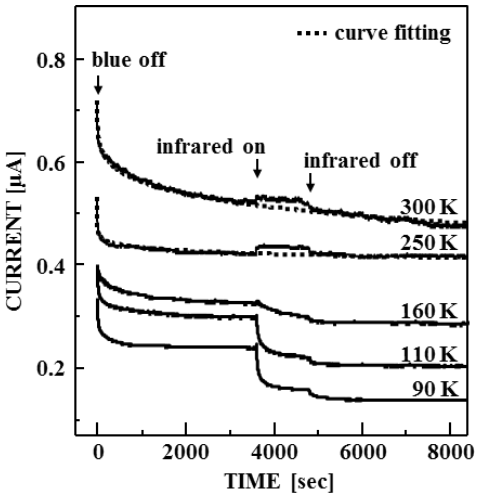

Fig. 2. PPC decay measured at various temperatures under the DLI. The fitting curves at 250 and 300 K show the least squares fit of data by the stretch-exponential function [3].

REFERENCES:

[1] A. Janotti, C.G. Van de Walle, Phys. Rev. B 76 (2007) 165202.
[2] S. Lany, A. Zunger, Phys. Rev. B 72 (2005) 035215.
[3] H.X. Jiang, J.Y. Lin, Phys. Rev. Lett. 64 (1990) 2547.
[4] T. Oga, Y. Izawa, K. Kuriyama, K. Kushida, and Q. Xu, AIP Conf. Proceedings, Vol. 1399, (2011) 67. 30th International Conference on the Physics of Semiconductors (Soule, Korea).

採択課題番号 23P8-1 化合物半導体の照射効果と電気的・光学的特性に関する研究 プロジェクト
(法政大院) 栗山一男、尾賀孝宏、伊田孝寛 (大阪教育大) 串田一雅
(京大・原子炉) 徐 虬

PR8-2

X-ray Diffraction Analysis of ZnO Implanted with Sn^+ at Room Temperature and 110 K

G. T. Dang, N. Nitta, M. Taniwaki, and T. Yoshiie[1]

Department of Environmental Systems Engineering, Kochi University of Technology
[1]Research Reactor Institute, Kyoto University

INTRODUCTION: Nowadays, II-VI compound semiconductors are noticed because of its potential applications in (opto)electronic devices. Particularly ZnO has regained research interest in the field of opt-electronic devices working in the blue and ultraviolet regions. However, wide applications have been impeded by difficulty in achieving p-type conductivity ZnO. Better understanding of defect structures is necessary to overcome this difficulty. Ion implantation, which is a standard technique in semiconductor device process at present, is an artificial way to produce defects in semiconductors. In this study, ZnO wafers were implanted with 60 keV Sn^+ ions. The wafers were examined by means of X-ray diffraction (XRD).

EXPERIMENT: 99.99% pure ZnO samples with dimensions of 10×10×0.54 mm^3 were implanted with 60 keV Sn^+ ions to doses of 2×10^{14}, 4×10^{14}, 8×10^{14}, and 1.5×10^{15} ions/cm^2 at room temperature (RT samples) and 4×10^{14}, 8×10^{14}, and 1.5×10^{15} ions/cm^2 at 110 K (LT samples). The zinc surface of the (0001) plane of all samples was implanted, except for the 2×10^{14} ions/cm^2 RT sample, whose oxygen surface was implanted. XRD patterns ($\theta-2\theta$ scan) were measured in these samples by an ATX Rigaku XRD-diffractometer using the Cu Kα line (λ=1.5418 Å).

RESULTS: In the wide-range XRD patterns of the unimplanted, 1.5×10^{15} ions/cm^2 RT, and 1.5×10^{15} ions/cm^2 LT samples, two strong peaks were observed at 34.42°, and 72.58°. These peaks correspond to 0002 and 0004 reflections, respectively. A weak peak at 52.70° was observed in all samples except for the 1.5×10^{15} cm^2 LT sample. This peak corresponds to the 0003 reflection. Its appearance indicates that these samples contained some defects (probably twins), because the 0003 Bragg reflection is forbidden in the wurtzite-type perfect crystals. The fine-scans of the 0002 peak for the unimplanted sample and all RT samples are illustrated in Fig.1 a. By implantation at room temperature, a broad line component appeared around the 0002 peak and its width increased with implantation dose. However the results for LT samples were different from RT samples. Figure1 b displays the fine-scans for the LT samples. The change with implantation dose was not discernible. This will be due to the difference in migration of the implantation-induced defects between RT and LT samples. Movement of the implantation-induced point defects depends on temperature; that is, the active migration of the implantation-induced defects at room temperature disturbs the lattice structures leading to the broadening of the reflected line.

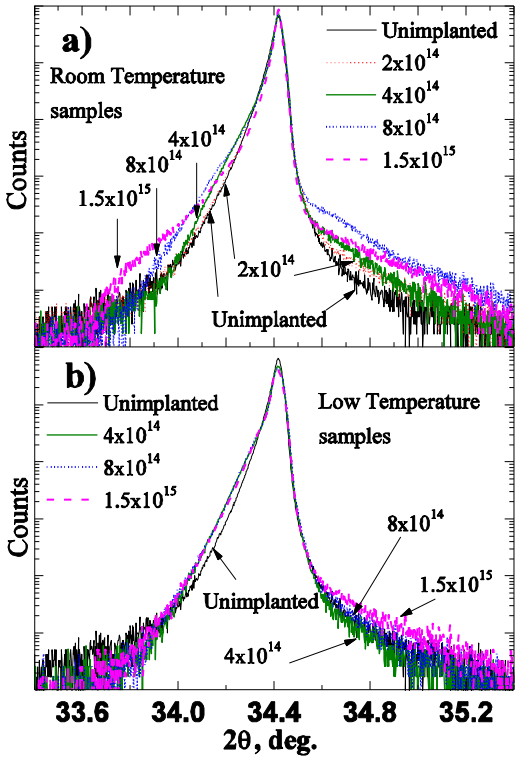

Fig.1 Fine-scans of the XRD 0002 peak: RT samples and b) LT samples. (Referred from G. T. Dang *et al.*, AIP Conf. Proc. 1321, 270 (2011))

採択課題番号23P8-2　半導体イオン照射によって導入される点欠陥挙動の解明とナノセル技術の開発　プロジェクト
（高知工科大）谷脇雅文、新田紀子、Dang Tchai Giang、石川　修、横山和弘、横田正博
（京大・原子炉）　義家敏正、徐　虬

PR8-3 Study on Formation and Recovery of Damage in Irradiated Crystalline Materials

A. Kinomura, K. Sato[1], Q. Xu[1] and T. Yoshiie[1]

National Institute of Advanced Industrial Science and Technology (AIST)
[1] *Kyoto University Research Reactor Institute (KURRI)*

INTRODUCTION: Radiation effects of ion irradiation have been extensively studied for various materials. Irradiation-induced damage degrades crystallinity and gives harmful effects on material properties. However, under appropriate irradiation or annealing conditions, the radiation and/or damaging effects can induce interesting effects and useful structures in materials. A typical case of such effects is the ion beam annealing in Si, where implantation-induced damage layers are recrystallized under other ion irradiation at elevated temperatures. Thus, it is important to investigate the radiation effects for the application and fundamental studies on interactions of energetic particles (ions and neutrons) with materials.

EXPERIMENTS: Two types of samples were studied in this year: (1) Hydrogen-implanted multicrystalline Si to observe the gettering of metal impurities to hydrogen-induced nanocavities; (2) ion-irradiated Ni to investigate the difference between the calculated ion range and the actual depth of damage. Some of these irradiated samples have been characterized by neutron activation analysis or positron annihilation spectroscopy. We performed cross-sectional transmission electron microscopy (TEM) to understand the nature of the radiation damage. It is difficult to make thinned samples for cross-sectional TEM observation, when the amounts of samples are limited. To obtain sufficient TEM samples from such samples, we used an FIB (focused ion beam) milling system. The FIB milling method is also good for multicrystalline samples like this study. The TEM observation was performed at an electron energy of 200 keV.

RESULTS: The multicrystalline Si observed was implanted with 50 keV H^+ to a dose of 3×10^{16} cm^{-2} and annealed at 850 ºC for 1h. Cross-sectional TEM samples were taken from the positions overriding grain boundaries as shown in Fig. 1(a). Pt protective layers were deposited on the sampling point (approximately 12 × 2 μm) prior to the cutting process to protect the surface side of the cross-sectional sample during the FIB milling. The thickness of the sample was about 2 μm at the beginning and further thinned by FIB milling. Fig. 1(b) shows the TEM image after the FIB milling. This image almost covers the whole area exposed to the ion milling (about 10 μm wide). A continuous band of nanocavities was clearly observed around the projected range of 50 keV H^+ (~0.5 μm) as shown in Fig. 1(b). The grain boundary should be at the middle of the observed region. However, interestingly, there was no influence of the grain boundary on the nanocavity band. TEM samples were also made from a pure Ni sample irradiated with 150 keV Ar^+ to a dose of 1×10^{15} cm^{-2} at room temperature. This sample was observed by EBSD (Electron BackScatter Diffraction) in advance. It is confirmed that the crystal grains observed in EBSD were precisely identified in SIM (secondary ion microscopy) images and the grains of interest can be chosen for the FIB milling method. The sampling of the TEM sample was successfully performed in the same way as the Si samples. We plan to perform electrochemical etching to remove the damage caused by the FIB milling.

In summary, the TEM sample preparation by the FIB milling was performed for multicrystalline-Si and pure-Ni samples in this study. The hydrogen-induced nanocavities were successfully observed for the Si samples around the grain boundary.

ACKNOWLEDGMENT: We would like to thank colleagues in AIST for their assistance on this study.

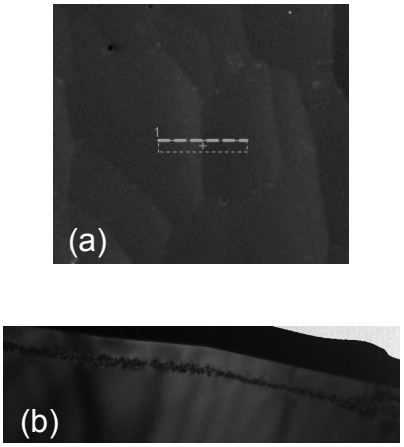

Fig. 1. Images of the multicrystalline Si sample after H-implantation and annealing. (a) Plan-view SIM image showing the sampling position for TEM. (b) Cross-sectional TEM image of the thin specimen obtained after milling.

採択課題番号 23P8-3　照射下の結晶材料における損傷形成と回復過程の研究　　プロジェクト
（産総研）木野村淳（京大・原子炉）佐藤紘一、徐　虬、義家敏正

PR8-4

Orange Emission of Calcites by Gamma Rays

T. Awata, T. Kishino, F. Maki and Q. Xu[1]

Department of Physics, Naruto University of Education
[1]Research Reactor Institute, Kyoto University

INTRODUCTION: The calcite ($CaCO_3$) has been studied since 1940's [1-3], because the intensity of thermoluminescence of calcite is higher than other famous minerals (e. g. fluorite) and it has the possibility of radiation dosimeter. V. Ponnusamy et al. [4] reported that the intensity of luminescence of calcite irradiated by gamma rays was depend on the annealing and the emission spectra have an emission band at 610nm (orange), and might be assumed that the recombination are always in involves Mn^{2+} ions. Last year, we reported thermoluminescence of natural calcite irradiated by gamma rays and it was shown that the spectra had only one orange emission peak at 620nm and that may be originated from impurity Mn^{2+}[5]. In this study, we have performed trace element analysis of natural calcite using NAA (Neutron Activation Analysis), XRF (X-ray Fluorescence Analysis) and ICP-AES (Inductively Coupled Plasma Atomic Emission Spectroscopy) to clear the relationship with orange emission bands and impurities of calcite.

EXPERIMENTS: The samples were some natural calcites and were irradiated neutron at Pn-3 of KUR for NAA. The gamma-rays spectra were taken by Ge detector at KUR after 1day for short-lifetime element and after two weeks for long-lifetime elements. ICP-AES (iCAP6300Duo, Themo Fisher) was also performed to measure element concentration of calcites at KUR. To analyze the element characterization of calcites, we had used XRF (Simultix 14, Rigaku).

RESULTS and DISCUSSION: Figure 1 shows the gamma-ray energy spectrum of typical natural calcite (Futagoyama, Saitama, JAPAN) irradiated by neutron at Pn-3 for after 1 day. It is shown that manganese, lanthanum and sodium were detected in the calcite. On the two weeks after measurements, no element without calcium was detected. Figure 2 shows the X-ray fluorescence spectrum of natural calcite. In this figure, it can be shown that manganese and iron are dominant impurities in the calcite. To clear the impurity concentration of the calcite, ICP-AES was performed. From the experimental results, impurities of manganese (57.1ppm), sodium (9.12ppm), iron (4.73ppm) and Copper (0.345ppm) are contained in calcite. At the all experimental results, Mn was always detected and was dominant impurity of calcite. V. Ponnusamy et al. had concluded the orange emission around 610nm is originated from the electron transition from ^4G to ^6S state of Mn^{2+}. In our results, thermoluminescence spectra of calcite has emission peaks at 620nm, and slight different from their results. We have to clear the reason this difference and influence of other impurities (especially Fe and Cu) in the near future.

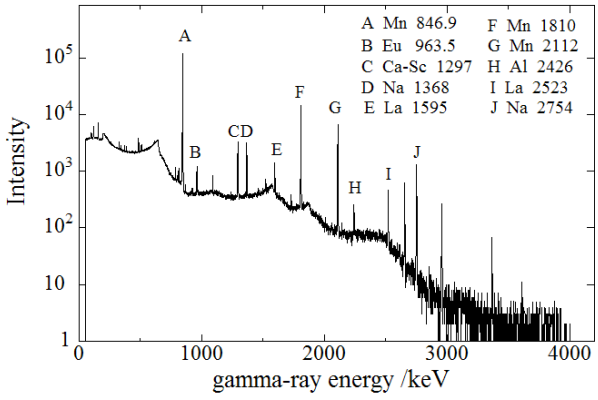

Fig. 1. Gamma-ray energy spectrum of natural calcite.

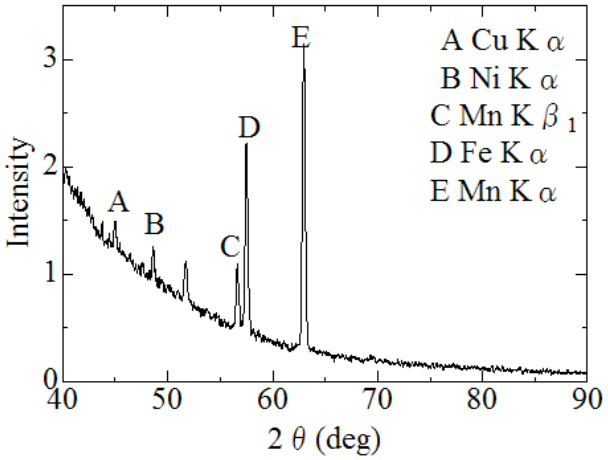

Fig.2 .X-ray fluorescence spectrum of calcite.

ACKNOWLEDGEMENT: We would like to thank Professor Dr. Fukutani (KURRI) for assistance on this study.

REFERENCES:

[1] W. L. Medlin, *J. Opt. Soc. Am.* 53(1963) 1276-1285.
[2] W. L. Medlin, J. Chem. Phys. **30**, pp451-458 (1959).
[3] W. L. Medlin, Phys. Rev, **135**, pp.A1770 (1964).
[4] V. Ponnusamy, V. Ramasamy, M. Dheenathayalu, et al., *Nucl. Instr. and Meth.* B **217** (2004)611-620.
[5] T. Awata and Q. Xu, KURRI Progress Report 2010 p.183.

採択課題番号 23P8-4　　高エネルギー粒子線による絶縁体の照射効果　　プロジェクト
（鳴門教育大学）粟田高明，岸野哲也，牧文哉（京大・原子炉）義家敏正，徐虫し

PR8-5 Annealing Behavior of Thermal Diffusivity and Positron Annihilation Lifetime in 30MeV Electron-irradiated Ceramics

M. Akiyoshi, I. Takagi, T. Yoshiie[1], Q. Xu[1] and K. Sato[1]

Faculty of Engineering, Kyoto University
[1]Research Reactor Institute, Kyoto University

INTRODUCTION:

Measurement of thermal diffusivity and positron annihilation lifetime were performed on 30MeV electron irradiated ceramics. In this study, electron irradiation was performed to 0.01 dpa via 30MeV KURRI-Linac. The electron irradiated specimens showed obvious degradation in thermal diffusivity and increment in positron annihilation lifetime. In addition, isochronal annealing was conducted every 100℃ up to 1100℃ in a vacuum. The annealing behavior of several specimens showed that positron annihilation lifetime gives good correlation with thermal diffusivity.

EXPERIMENTS:

Typical structural ceramics (α-Al_2O_3, AlN, β−Si_3N_4 and β-SiC) were irradiated by 30MeV electron using the KURRI-LINAC up to $1.5x10^{24}e/m^2$ (correspond to 0.01dpa) at 300K in the water-cooled specimen holder. Thermal diffusivity was measured by laser flash method at the room temperature, and as-irradiated specimen showed about 20%, 40%, 30%, 75% degradation in α-Al_2O_3, AlN, β-Si_3N_4 and β-SiC respectively.

Positron annihilation lifetime was also measured using conventional γ-γ fast coincidence method in Radiation Laboratory, Uji. The irradiated specimen was a ϕ10x0.5mm disk. Positron source was specially ordered 1MBq ^{22}Na sealed by Ti foil, and the active diameter was 1mm.

The obtained PAL spectrum was analyzed with PALSfit program, with FWHM about 230ps. In analyze of the spectrum, a source component that represents annihilation in the Ti foil was not resolved, and only two or three component was guessed in the analysis.

After the measurement for the as-irradiated specimens, isochronal annealing was conducted every 100℃ up to 1100℃ in a vacuum. After the each step of annealing, specimens were cooled to the room temperature and then thermal diffusivity and PAL measurements were performed at the room temperature.

RESULTS:

After the spectrum analysis, average positron lifetime $<\tau>$ was obtained as $<\tau> = \tau_1 I_1 + \tau_2 I_2$, where τ_i are the analyzed positron lifetimes and I_i are the intensities for the components. The average lifetime $<\tau>$ of electron irradiated α-Al_2O_3 and AlN indicated significant increment same as neutron irradiated specimens. On the other hand, β-Si_3N_4 and β-SiC showed almost no change in lifetime same as neutron irradiated specimen.

The annealing behavior of PAL showed almost same trend as that of thermal diffusivity in α-Al_2O_3 and AlN. On the other hand, PAL in β-Si_3N_4 and β-SiC showed different behavior from the thermal diffusivity. This trend fit to the correlation between thermal diffusivity and PAL measured for specimens irradiated several different conditions in the previous work.

AlN showed most clear correlation between thermal diffusivity and PAL during the annealing. On the other hand, the thermal diffusivity of unirradiated α-Al_2O_3 specimen was no so high, so the annealing behavior was not clear. β-SiC specimen showed clear recovery in thermal diffusivity but the specimen was p-type SiC, therefore the PAL did not show obvious change after the irradiation and the annealing. Now n-type SiC was irradiated using the LINAC, and it is expected that the specimen show clear correlation even in a covalent bond ceramics.

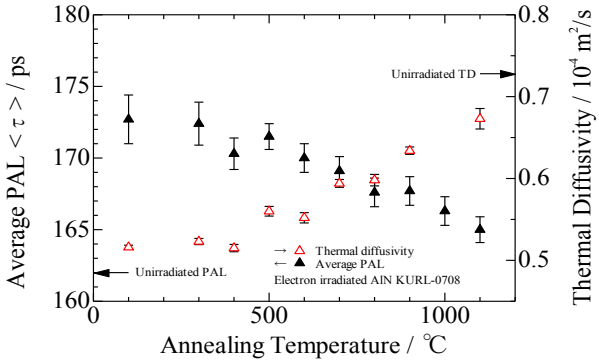

Fig 1: Annealing behavior of thermal diffusivity and PAL in electron-irradiated AlN.

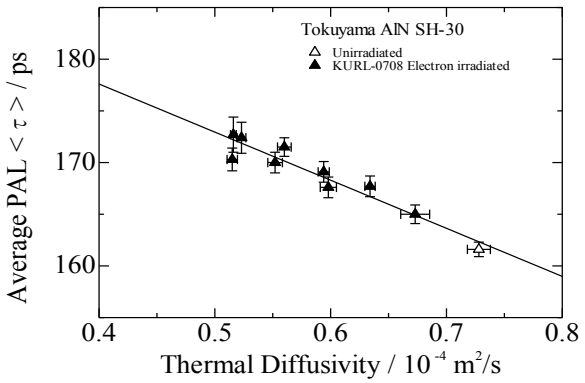

Fig 2: Correlation between thermal diffusivity and PAL obtained from an electron-irradiated AlN specimen with isochronal annealing.

採択課題番号 23P8−5　照射セラミックスの熱拡散率及び陽電子消滅法による欠陥評価　プロジェクト
（京大・工）秋吉 優史、高木 郁二（京大・原子炉）義家 敏正、徐 虬、佐藤 紘一

PR8-6 Defects in a Zr-Nb Alloy Studied by Positron Annihilation and Atom Probe Tomography

Y. Nagai, T. Toyama, Y. Matsukawa, Y. Shimizu, A. Kuramoto, H. Takamizawa, Y. Kakubo, K. Inoue[1], T. Yoshiie[2], Q. Xu[2], K. Sato[2]

Institute for Materials Research, Tohoku University

[1]*Department of Materials Science and Engineering, Kyoto University*

[2]*Research Reactor Institute, Kyoto University*

INTRODUCTION: Zr-Nb alloy is an advanced nuclear material recently developed for fuel cladding tubes that store uranium pellets in light-water nuclear reactors operated at extended fuel burn-up rates such as 65~70 GWdt-1, which is 20~30% greater than the current standard, for improving economic efficiency. The origin of the excellent properties on corrosion resistance and suppression of hydride formation considered to be related to Nb precipitates, however the detail is not understood yet. In this work, we employed positron annihilation and atom probe tomography (APT) to study the defects related to the Nb precipitates in Zr-Nb alloy.

EXPERIMENTAL: The samples used in this study are an Zr-1.8wt%Nb alloy. A part of the samples were irradiated at 77K by 28MeV electrons to a fluence of about 5×10^{18} e/cm^2 using the KUR-LINAC.

RESULTS & DISCUSSION: Fig. 1 shows positron coincidence Doppler broadening (CDB) ratio spectra for the unirradiated and the electron-irradiated Zr-Nb normalized by pure-Zr. CDB ratio spectra for pure Nb and Fe are also shown as references. For the unirradiated sample, a broad peak around 18×10^{-3}mc is clearly observed. This peak originates from positron annihilation with Fe electrons which is contained as impurities in Zr-Nb alloy due to zirconium's high chemical reactivity. Judging from the peak height, the fraction of positrons annihilated with Fe electrons was estimated to be about 30 at.%. On the other hand, for the irradiated sample, such a broad peak around 18×10^{-3}mc is not observed as shown in Fig. 1. Fig. 2 shows mean positron lifetime for the unirradiated and the electron-irradiated Zr-Nb. In the electron-irradiated sample mean positron lifetime is almost same as that for vacancy in Zr, which indicates that positrons are mainly trapped at the vacancies in the Zr matrix introduced by the electron-irradiation. Fig. 3 shows APT elemental maps for the unirradiated sample. Fe segregation on the interface between Zr matrix and a Nb precipitate is clearly observed.

These results of positron annihilation and APT strongly suggest that positrons are mainly trapped at the precipitate-matrix interface decorated with Fe atoms for the unirradiated sample, while for the irradiated sample positrons are mainly trapped at the irradiation induced vacancies in the Zr matrix rather than the precipitate-matrix interface, because the vacancies are more abundant and attractive than the precipitate-matrix interface for positrons. This is consistent with the result that broad peak originated from positron annihilation with Fe electrons is not observed for the irradiated sample.

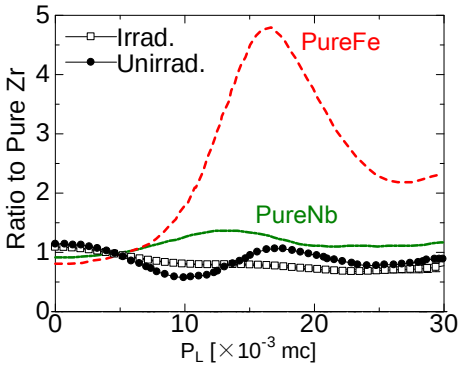

Fig. 1. CDB ratio spectra for the unirradiated and electron-irradiated Zr-Nb normalized by pure-Zr. CDB ratio spectra for pure Nb and Fe are also shown as references.

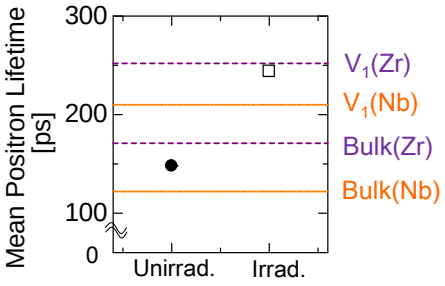

Fig. 2. Positron lifetime results for the unirradiated and electron-irradiated Zr-Nb.

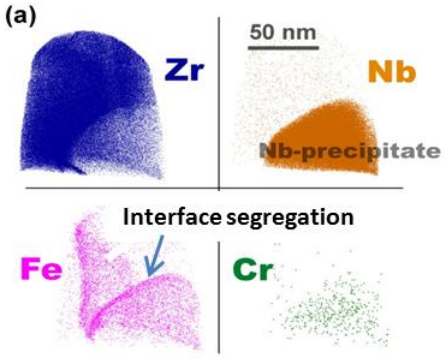

Fig. 3. APT elemental maps for the unirradiated Zr-Nb.

採択課題番号 23P8-6　　陽電子消滅および 3 次元アトムプローブによる低温照射効果の研究　　プロジェクト

（東北大・金研）永井康介、外山健、松川義孝、清水康雄、蔵本明、高見澤悠、鹿窪勇太（京大・工学研究科）井上耕治（京大・原子炉）義家敏正、徐虬、佐藤紘一

PR8-7 **Defects Study for Iron Alloys Damaged by Electron Irradiation**

F. Hori, M. Maruhashi, N. Onodera, A. Ishii, S. Mineno, A. Iwase, Q. Xu[1], K. Sato[1] and T. Yoshiie[1]

Dept. of Mater. Sci., Osaka Prefecture University
[1]*Research Reactor Institute, Kyoto University*

INTRODUCTION: It is well known that the irradiation damage of the metal under high-energy particles irradiation makes various effects with the alloy compositions. Especially, the mechanism of radiation embrittlement in the pressure vessel steels of the light water reactor is one of the most important subjects which are related to the lifetime extension of the nuclear reactors. The embrittlement of the pressure vessel steels during irradiation is partly due to copper precipitation, many researches of the irradiation effect about the precipitation process of copper atom in the solid solution of Fe-Cu alloy have been studied in the past. However, copper precipitation is previously formed in the welding part in the reactor pressure vessel, and there are few discussions on the irradiation effect for existing Cu precipitation.

EXPERIMENTS: The specimens were annealed at 850℃ for 2 hours, followed by quenching into 0℃ water, then the Fe-Cu alloys with the copper concentration of 0.6 and 1.2 wt.% forming solid solution were prepared. Moreover, the Fe-Cu alloys were aged at 500℃ for 48 hours, in order to form Cu precipitation in the iron matrix. These specimens were irradiated 30 MeV electrons at 77K up to 5.0×10^{17} e^-/cm^2 and 1MeV neutrons at 4K using the research reactor at Kyoto University Research Reactor Institute. Electrical resistivity in-situ measurement has been performed for neutron irradiation at 4 K during irradiation. After irradiation, electrical resistivity and positron annihilation measurements have also been performed.

RESULTS: The results of electrical resistivity measurement show that the electrical resistivity increases by the electron and neutron irradiation, and the change in resistivity in solid solution alloy is larger than that in same alloy including Cu precipitation. This result suggests that the dissociation of some Cu precipitation occurred. In general, irradiation induced point defects make Cu atoms aggregation in Fe-Cu alloys with solid solution. Fig. 1 shows the electric resistivity change, which is normalized by the value before irradiation, for each Fe-Cu alloy during neutron irradiation. In this figure, neutron flux increases with constant rate until 3800 sec and becomes constant after that. In case of neutron irradiation, it appears the different trend of change in the electrical resistivity between these alloys. This difference may come from the dissociation of some Cu precipitation and the local re-precipitation of dissociated Cu atoms occurred in balance. These phenomena inhibited the increase of electrical resistivity by neutron irradiation.

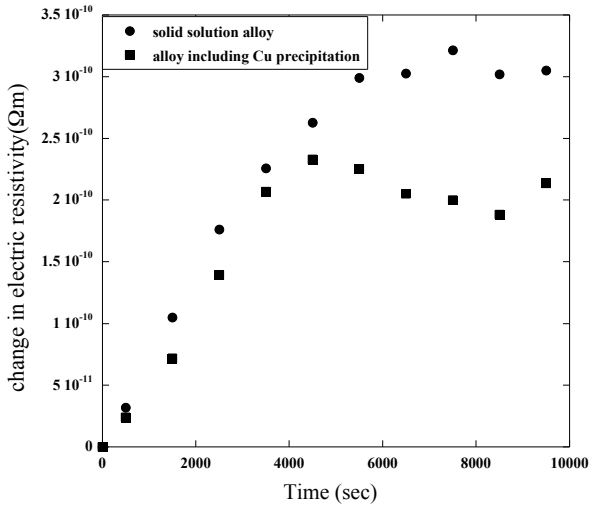

Fig. 1 Change in electric resistivity for solid solution and annealed (Cu precipitation formed) alloys during neutron irradiation.

採択課題番号 23P8-7　　金属合金における照射効果の研究　　プロジェクト
（阪府大・工）堀史説、丸橋基邦、小野寺直利、石井顕人、峯野慎也、岩瀬彰宏
（京大・原子炉）徐虬、義家敏正、佐藤紘一

PR8-8 Recovery Process of Neutron-Irradiated Vanadium Alloys in Post-Irradiation Annealing Treatment

K. Fukumoto, M. Iwasaki[1] and Q. Xu[2]

RINE, Univ. of Fukui
[1] Graduate school of Eng., Univ. of Fukui
[2]KUR, Kyoto Univ.

INTRODUCTION:

In this study, experiments to determine the post-irradiation annealing effect on the mechanical properties and microstructures of neutron-irradiated V-Cr-Ti were conducted in this study. Two groups of specimens (as-irradiated specimens and specimens which underwent the post-irradiation annealing treatment) were subjected to tensile tests at room temperature and 500°C. Post-irradiation annealing experiments were carried out for long periods (up to 50 hrs) in an effort to restore the original strength and ductility. In order to understand the thermal stability of the defect clusters, and investigate a recovery method for irradiation hardening and embrittlement, post-irradiation annealing experiments were performed to evaluate the recovery of the microstructure and mechanical properties of vanadium alloys irradiated below 300°C.

EXPERIMENTS: The majority of test specimens for this study were prepared from V-4Cr-4Ti alloys. The tensile specimens had nominal gauge dimensions of 0.25mm(t) x 1.2mm(w) x 5mm(l). Before irradiation, all specimens were annealed in vacuum at 1000°C for 2hrs. The specimens were irradiated at 228°C to 280°C with 3 to 5 di splacements per atom (dpa) in the ATR-A1. Post-irradiation annealing was carried out for 2 to 50 hr at 500°C and 600°C in a vacuum. Tensile tests were conducted at room temperature and 500°C. TEM samples were punched from non-deformed areas of tested specimens. The microstructural TEM observations were performed in KUR/Kyoto Univ.

RESULTS: Tensile behavior was reported in the last KURRI progress report 2010. From TEM observation, the density of defect clusters was very high and the size of each cluster was very small, about a few nm, in the as-irradiated specimens. With increasing annealing time at 500°C, the density of defect clusters decreased gradually. The clusters grew into large dislocation loops on annealing for 50 hrs at 500°C. With increasing annealing time, the density of defect clusters showing as black dots decreased and the defect clusters grew into dislocation loops. The yield stress increases were estimated by analyzing the microstructural changes. This estimation was carried out using the well-known dispersed barrier hardening equation,

$$\Delta\sigma y = M\alpha\mu b(Nd)^{1/2} \quad (1)$$

where $\Delta\sigma y$ is the increase in strength from the unirradiated value, μ is the shear modulus, and b is the magnitude of the a/2[111] Burgers vector of the dislocation loops; N and d are the density and size of the defect clusters, respectively; M is the Taylor factor, which is set to M=3. The calculated value of the barrier strength for the dislocations was 0.35 according to the previous data revised using the M=3 estimation. Fig.1 shows the comparison of yield stress increases estimated from the experimental results and microstructural analyses as a function of annealing time. The estimated values of yield stress increase were consistent with the experimental results and the irradiation hardening corresponded to the microstructural changes due to the neutron irradiation and the following post-irradiation annealing treatment. In the case of the as-irradiated sample, the fracture of the tensile specimen occurred before the stress level reached the ultimate tensile stress; that is, a plastic instability due to local propagation of the deformation proceeded and it was considered that the stress increase was underestimated in the experimental data.

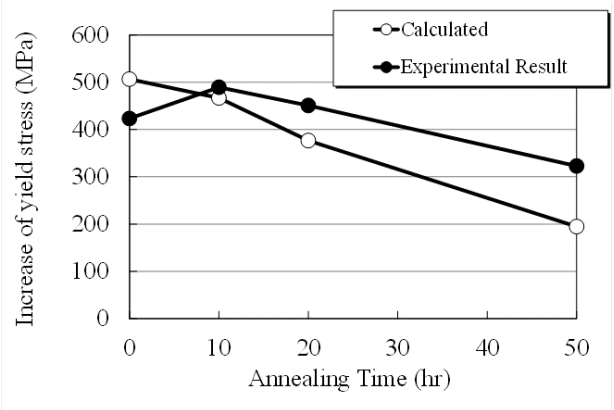

Fig. 1. Comparison of yield stress increases estimated from experimental results and microstructural analyses, as a function of annealing time for the post-irradiation annealed V-4Cr-4Ti alloys

採択課題番号 23P8-8　　中性子・イオン照射を用いたバナジウム合金の熱処理による損傷回復過程　　プロジェクト研究

（福井大院工）福元　謙一、岩崎将大　（京大・原子炉）徐　虫Ｌ

PR8-9

Damage Evolution in Neutron-irradiated Metals during Neutron Irradiation at Elevated Temperatures

I. Mukouda*, K. Yamakawa[1], T. Yoshiie[2] and Q. Xu[2]

Hiroshima International University
[1]*Faculty of Engineering, Ehime University*
[2]*Research Reactor Institute, Kyoto University*

INTRODUCTION: A structural ordering of atoms in Au_3Cu alloy has been investigated by the electrical resistivity measurements. The isochronal resistance curve has been investigated experimentally during ordering and disordering. In many investigations the electrical resistance of the specimen was measured *in situ* at constant rate of heating but it was not measured isochronally at the same temperature. In the present experiment the electrical resistances of the Au_3Cu alloy are measured isochronally at 3 constant temperatures during ordering and disordering for various heating treatments.

EXPERIMENTS: Two types of specimen were prepared in the present experiment. One of which was the quenched specimen from 400°C and the other was the fast cooled specimen from 230°C or 250°C.

On the quenching, the specimens were quenched from the high temperature by falling down into water in a vertical furnace with flowing Ar+3%H_2 gas mixture. On the fast cooling, the stainless steel tube, in which the specimen was set, filled with helium gas was quenched into ice water. The fast cooling rate of the specimen from 230~250°C was 15~30°C/sec.

The electrical resistance was measured isochronally at 3 constant temperatures (ice water temperature, liquid nitrogen temperature and liquid helium temperature) during the annealing. The heating rates were 10K/20min, 10°C/100min and 10°C/300min for the quenched specimen, and 10°C/100min for the fast cooled specimen, respectively.

RESULTS: The isochronal resistance curves with different heating rates, for the quenched specimen from 400°C is shown in Figs.1(a)~(b) for various measuring temperatures, respectively. The measuring temperatures are 0°C(Fig.1(a)) and liquid helium temperature(Fig.1(b)). The resistance in Fig.1 increases with the temperature and then decreases around the critical temperature. The curve shifts to high temperature side with heating rate. The curves at 10°C/300min do not bend smoothly but bend clearly as composed by two stages. The dissociation to two stages of the resistance curve during ordering is first observed in this isochronal curve at low heating rate. This dissociation becomes clear with lowering of the measuring temperature.

The isochronal resistance curves of the fast cooled specimen from 250°C are shown in Figs.2(a)~(b) together with the resistance curves of the quenched specimen for various measuring temperatures. The measuring temperatures are 0°C(Fig.2(a)), and liquid nitrogen temperature and liquid helium temperature(Fig.2(b)). It must be noted that the resistance maximums of fast cooled specimen appear at the same annealing temperatures for the main maximums of quenched specimen and sub-maximums as in quenched specimen are not found. Even at this low heating rate such as 10°C/100min the curve increases smoothly and does not dissociate to two stages different from the quenched case. The excess vacancies obtained by the quenching would enhance the ordering by help atomic diffusion during the isochronal annealing. However the excess vacancies would be gradually consumed during the annealing at low heating rate and would become to equilibrium value.

Therefore, the rate of resistance increase would be slow down at one time and be appeared 2 stages like change in the resistance. In fact, the number of atomic jumps, at 120°C in the quenched specimen is roughly the same order of magnitude at 180°C in the quenched specimen and the fast cooled specimen.

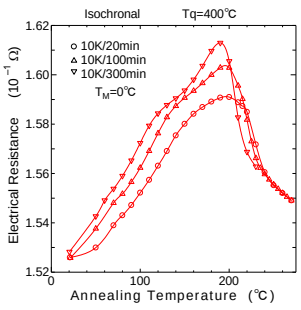

Fig. 1(a)

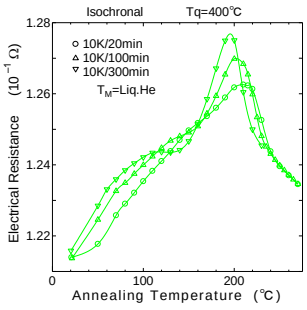

Fig. 1(b)

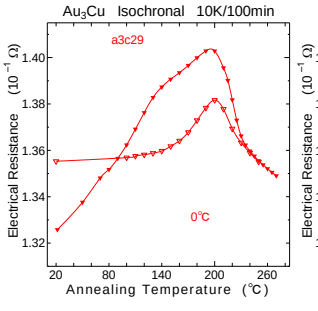

Fig. 2(a)

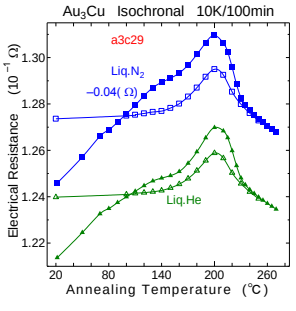

Fig. 2(b)

採択課題番号 23P8-9　　高温での中性子照射金属中の点欠陥集合体動的挙動と損傷組織発達過程　　プロジェクト

（広島国際大学）向田一郎、（愛媛大）山川浩二、（京大原子炉）　義家敏正、徐　虬

PR8-10 Effects of Thermal Aging and Irradiation on Mechanical Properties of Fe-Cr Ferritic Alloys

R. Kasada, Y. Sakamoto, K. Yabuuchi, A. Kimura,
K. Sato[1], Q. Xu[1] and T. Yoshiie[1]

Institute of Advanced Energy, Kyoto University
[1]Research Reactor Institute, Kyoto University

INTRODUCTION: Fe-Cr binary system is an important basis for the structural materials of energetic power plants such as fossil fuel ones, next generation fission reactors and fusion reactos. However, such high-Cr steels may suffer from thermal aging embrittlement, which is well-known 475 °C embrittlement, due to phase separation of Fe and Cr. Recently, Kasada and Sato are widely investigating the positron trapping behavior in the Fe-Cr alloys under "the Strategic Promotion Program for Basic Nuclear Research by the Ministry of Education, Culture, Sports, Science and Technology of Japan". So the present collaborative research has moved to investigate the neutron irradiation effect on the phase separation of Fe-Cr ferritic alloys. In the FY2011 we have irradiated the Fe-Cr alloys in KUR. The post-irradiation experiments including hardness test and positron annihilation spectrometry will be done in FY2012.

Here, we reports the ion-irradiation results for the Fe-Cr alloys as a reference data for the neutron irradiation in KUR

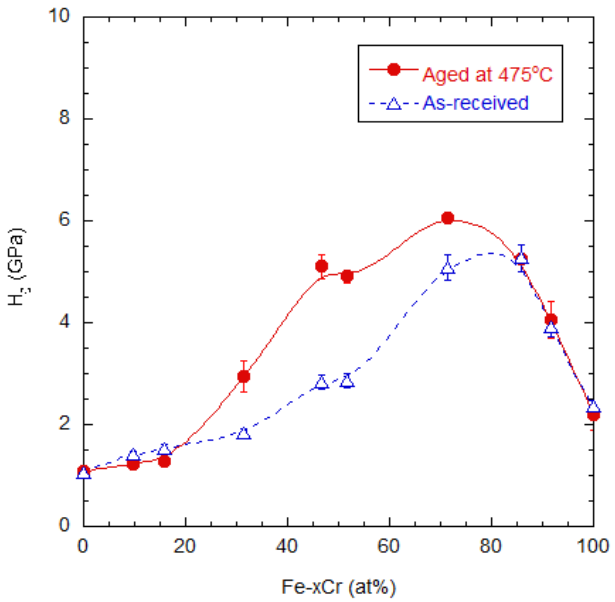

Fig. 1. Cr-dependence of a bulk-equivalent hardness, H_0, converted from nano-indentation hardness of Fe-Cr binary alloys [1].

Experimental Procedure: Materials used in the present study is Fe-Cr binary alloys (Fe-xCr; x = 0, 0.09, 0.16, 0.31, 0.47, 0.51, 0.70, 0.84, 1). Thermal aging treatment on these materials was carried out at 475 °C up to 100 h. Some of the materials were ion-irradiated at 290 °C up to 5 dpa, in DuET facility, Institute of Advanced Energy, Kyoto University. Nano-indentation hardness tests were performed using Nano-Indenter G200 with a continuous stiffness measurement method to obtain the hardness depth profile.

Results and Discussions: As previously shown in the Fig. 1 [1], the Cr-dependence of the H_0 is very similar to that of the micro-Vickers hardness obtained for the similar materials. The depth-dependence of the nanoindentation hardness of ion-irradiated Fe-9Cr were analyzed using the extended Nix-Gao model [2]. These data sets will be provided for the reference data of the following neutron irradiation experiments in KUR.

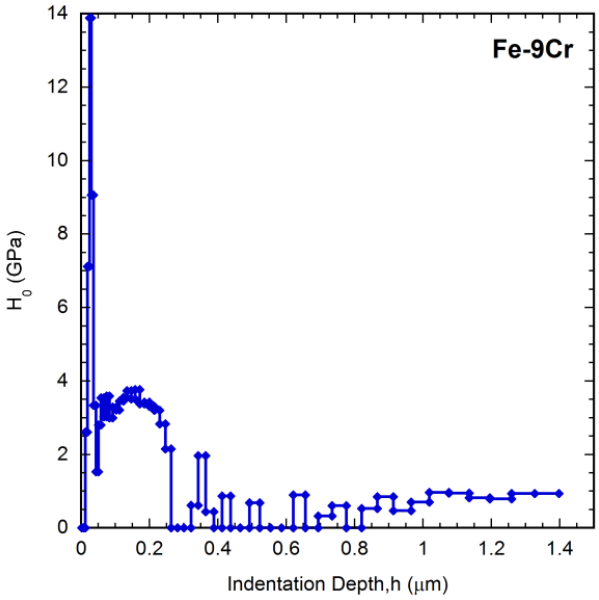

Fig. 2. Depth-dependence of a bulk-equivalent hardness, H_0, converted from nano-indentation hardness of ion-irradiated Fe-9Cr binary alloy.

REFERENCES

[1] R. Kasada et al., KURRI progress report 2010. 1
[2] W. D. Nix and H. Gao: J. Mech. Phys. Solids 46 (1998), p. 41

採択課題番号 23P8-10　　Fe-Cr 合金の相分離に及ぼす照射効果　　プロジェクト
（京大・エネ研）笠田　竜太、木村晃彦、藪内聖皓、坂本雄太
（京大原子炉）佐藤　紘一、義家　敏正、徐　虬

PR8-11 **Radiation Resistance of Nanocrystalline Ni by Neutron Irradiation**

H. Tsuchida, A. Itoh[1], K. Satoh[2], T. Yoshiie[2] and Q. Xu[2]

Quantum Science and Engineering Center, Kyoto University
[1]Depertment of Nuclear Engineering, Kyoto University
[2]Research Reactor Institute, Kyoto University

INTRODUCTION: Studies of radiation resistance of nuclear reactor materials are of technological importance to perform evaluation of age-related deterioration of the materials. Irradiation induces production of radiation defects and their accumulation, resulting in a change of microstructure in materials. It is well known that a nanocrystalline material with grain size of less than a few tens micrometers has high resistance to radiation damaging effects. This is due to the fact that grain boundary acts as effective sinks that absorb radiation-induced defects. A recent simulation study has showed a new mechanism of radiation resistance in nanocrystalline materials: self-healing of radiation damage occurs via interstitial emission near grain boundary, resulting in suppression of defect accumulation [1].

In this work, radiation damaging effects in nanocrystalline Ni under neutron irradiation were studied. Defect microstructure was analyzed by conventional positron annihilation lifetime spectroscopy.

EXPERIMENTS: Samples were nanocrystalline (NC) Ni with an average grain size of about 30 nm, which was measured by a TEM observation. The samples were irradiated with neutrons from KUR operated at 1 MW. To investigate microstructure of the sample after irradiation, we performed measurements of positron annihilation lifetime spectroscopy (PALS) as a function of displacement per atom (dpa) estimated from neutron fluence, ranging from 3.8×10^{-5} to 1.8×10^{-3}. We also performed the same experiment for coarse-grained polycrystalline Ni annealed at 1523 K for 1 h under a high vacuum condition.

RESULTS: Figure 1 shows results of dpa-dependence of positron lifetime for NC Ni. Positron lifetime spectra were analyzed by two components τ_1 and τ_2, where the first lifetime τ_1 is attributed to positron trapping at the free volumes in the crystalline interfaces and the second lifetime τ_2 is due to the free volumes at the intersections of two or three crystallites interfaces. It is seen that the values of τ_1 remain unchanged with increasing the dpa, while the τ_2 increases slightly at above 4.6×10^{-4} dpa. The former result indicates that defect accumulation at crystalline interfaces is strongly suppressed under irradiation. The latter suggests that microstructure of free-volume at intersections changes with increasing the dpa. From these results, we concluded that radiation resistance of NC materials is related with no change in microstructure of crystalline interface.

Comparing results for NC Ni and coarse-grained counterpart, we found that a completely different dpa-dependence of the positron lifetime is observed depending on grain size: for the coarse-grained specimen, the lifetime increase monotonically with increasing the dpa. This is due to defect accumulation or formation of defect cluster.

In order to understand interface-microstructure of NC materials after irradiation in more detail, it is necessary to perform further experiment by combined analysis of Thermal desorption spectroscopy and Positron lifetime spectroscopy.

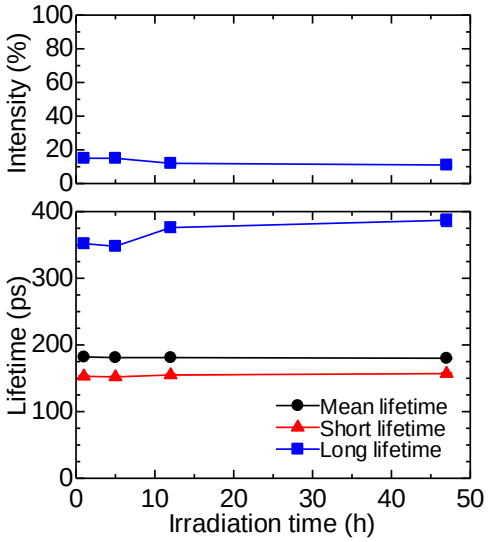

Fig. 1. Experimental results of positron lifetime as a function of dpa, where dpa per 1 h was 3.8×10^{-5}.

REFERENCES:

[1] Bai *et al.*, "Effective annealing of radiation damage near grain boundaries via interstitial emission", Science 327 (2010) 1631

採択課題番号 23P8-11　　水素イオン照射に伴う材料欠陥生成挙動の陽電子解析に関する研究　　プロジェクト

（京大院工）土田秀次、伊藤秋男（京大・原子炉）義家敏正、徐　虬、佐藤紘一

PR8-12 **Interaction between Deuterium and Defects in Tungsten**

K. Sato, R. Tamiya[1], Q. Xu and T. Yoshiie

Research Reactor Institute, Kyoto University
[1]Graduate School of Engineering, Kyoto University

INTRODUCTION: In a fusion reactor, plasma-facing materials (PFMs) must withstand the damage produced by hydrogen and helium at up to 10 keV of energy and heat loads from the plasma, in addition, the neutrons with high energy, high flux and high fluence similar to the structural components. Hydrogen isotopes retain in vacancy-type defects in PFMs, and this is a critical problem for fusion reactors. To know the interaction between vacancy-type defects and hydrogen isotopes is very important. In this study, the size and density of vacancy-type defects in tungsten was obtained by positron annihilation lifetime (PAL) measurements. Next, thermal desorption spectra of deuterium was obtained after deuterium charging. From these results, trapping site and dissociation energy of deuterium were identified.

EXPERIMENTS: The samples were 99.95% pure tungsten (A.L.M.T. Corp.). The 0.2-mm-thick sheet was punched to 5mm in diameter. These samples were annealed at 1773 K for 1 h in a vacuum of less than $10^{i\,4}$ Pa. Electron and deuterium ion irradiations were carried out to introduce defects. Electron irradiation of 8 MeV was performed at Electron Linear Accelerator of Research Reactor Institute, Kyoto University. Deuterium ion irradiation was performed at Low-energy ion irradiation system of Research Reactor Institute, Kyoto University. 5 keV D_2^+ ions were irradiated up to 1.0×10^{18} /cm^2 (20 dpa at defect peak) at room temperature (R.T.) and 673 K. A displacement threshold energy used for irradiation dose calculation was 42 eV [1]. After that, 1 keV D_2^+ ions, which do not induce irradiation defects, were implanted by low-energy ion irradiation system. Thermal desorption spectroscopy (TDS) was carried out from R.T. to 1523 K in order to detect elimination behavior of deuterium from tungsten.

RESULTS: TDS spectra of 8 MeV electron- and 5 keV D_2^+ ion-irradiated samples are shown in Fig. 1. The spectrum of sample annealed at 1273 K for 5 hours, which mainly includes dislocations, is also shown in Fig. 1. Because single vacancies are mainly formed by electron irradiation, a peak around 550 K denotes elimination of deuterium from single vacancies. Peak separation analysis was performed to spectra of 5 keV D_2^+ ion irradiation by data analysis software Origin, and the results were shown in Fig. 2 and 3. Spectra of 5 keV D_2^+ ion irradiation at R.T. and 673 K were resolved into three gauss functions. Peak of them is around 450 K, 560 K and 640 K. 450 K peak denotes the elimination of deuterium from surface. It is expected that 560 K peak denotes the elimination of deuterium from single vacancies from result of electron-irradiated sample. Because 5 keV D_2^+ ion irradiation is likely to form small vacancy clusters, the peak around 560 K may include the elimination from small vacancy clusters. This possibility is considered in next step. 640 K peak denotes the elimination of deuterium from dislocations, because the peak was obtained in sample annealed at 1273 K for 5 hours.

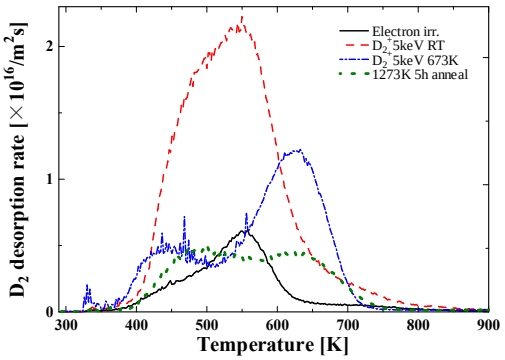

Fig. 1. TDS spectra of 8 MeV electron- and 5keV D^{2+} ion- irradiated and annealed samples.

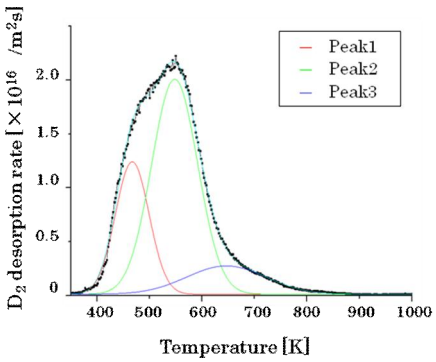

Fig. 2. Peak separation of TDS spectrum of sample irradiated with 5 keV D^{2+} ions at R.T.

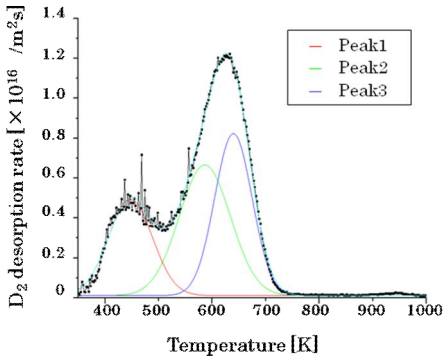

Fig. 3. Peak separation of TDS spectrum of sample irradiated with 5 keV D^{2+} ions at 673 K.

REFERENCES:

[1] F. Maury, M. Biget, P. Vajda, A. Lucasson and P. Lucasson, Radiat. Eff. 38 (1978) 53.

採択課題番号 23P8-12　電子照射された金属の損傷組織の照射温度依存性の研究　　プロジェクト
（京大・原子炉）佐藤紘一、徐虬、義家敏正（京大院・工）田宮怜

PR8-13 Irradiation Effects on Stress Loading Property of Refractory Metal at high Temperature

K. Tokunaga, K. Araki, T. Fujiwara, T, Hotta[1],
Q. Xu[2] and T. Yoshiie[2]

Research Institute for Applied Mechanics, Kyushu University
[1]Interdisciplinary Graduate School of Engineering Sciences, Kyushu University
[2]Research Reactor Institute, Kyoto University

INTRODUCTION: Tungsten is one of refractory metal and will be used as armor material of the first wall/blanket and divertor in the fusion reactor because of its low sputtering yield and low hydrogen retention. The plasma facing armor materials will be subjected to high flux bombardment of low energy particles including the hydrogen fuel and helium ash. In addition, stress by disruption and ELMs will be loaded on the armor material of the first wall/blanket and divertor of at high temperature. This is a concern because it is well known that helium implanted in tungsten does not release until high temperatures, due to strong interaction with lattice defects. Helium drastically enhances the formation of bubbles due to the strong bonding to vacancies and their clusters. As a result, local swelling and degradation of mechanical properties of bulk materials take place. It is anticipated that implanted helium influences the response of tungsten to stress loading at high temperature by the pulsed high heat loading such as disruption and ELMs. Very little information is available on the combined effects of helium implantations and the pulsed high heat loading. In the present work, helium pre-implanted tungsten has been exposed to pulsed electron beams to examine synergistic effects of helium irradiation and stress loading at high temperature by the pulsed high heat loading.

EXPERIMENTS: Tungsten samples used in the present experiment are powder metallurgy tungsten. The sample sizes and purity are 20 mm x 20 mm x 5 mm and 99.99%, respectively. The sample surface was mechanically and electrochemically polished. Helium beam irradiations were performed in an ion beam facility. The samples were mechanically mounted on a Cu holder which was actively water cooled. The helium energy was 18.7 keV. The helium beam flux and heat flux at the beam center was 2.0 x 10^{21} He/m^{2}s and 6.0 MW/m^2, respectively. The beam duration was 2.8–3.0 s. The samples were irradiated to a fluence between 10^{23} ～ 10^{24} He/m^2 by 130–150 pulse irradiations cycles. The beam diameter on samples was 16 mm, defined using apertures. The surface temperature of the sample was measured with a two-color optical pyrometer and the two dimensional surface temperature distribution of the samples was also monitored with an IR camera. After the helium irradiation, the samples were exposed to pulse heat loading by electron beam irradiation. The heat flux was 1 GW/m^{2,} with duration of 1, 1.5 or 2 ms. The half width value of the electron beam was 8 mm. The electron beam area on the tungsten surface was defined by a beam limiter with an aperture of 4 mm. The net electron current induced by the electron beam irradiation was also measured, the electron beam energy was 70 keV, and the heat flux was measured by the calorimetric method. Before and after the helium and electron beam irradiation, the sample surfaces were examined using a scanning electron microscope (SEM).

RESULTS: As shown in Fig. 1, formation of blisters, exfoliation and small pin hole are observed in boundary area of melted and non-melted zone. These surface modifications are considered to be due to the formation, coalescence and migration of helium bubbles near the surface under stress loading at high temperature during the pulse high heat loading of 1 ms. In addition, the pin holes may be formed by the migration of helium bubbles to the surface at a high temperature. On the other hand, surface smoothing at high temperature did not occur; however, partial exfoliation of blister caps with a diameter of about 1 μm and cracking along grain boundaries are formed in the non-melted zone on the electron beam irradiated area. It is possible that helium implantation in tungsten suppresses the migration of atoms at high temperature because radiation damage, such as helium bubbles act as obstacle to the atom migration.

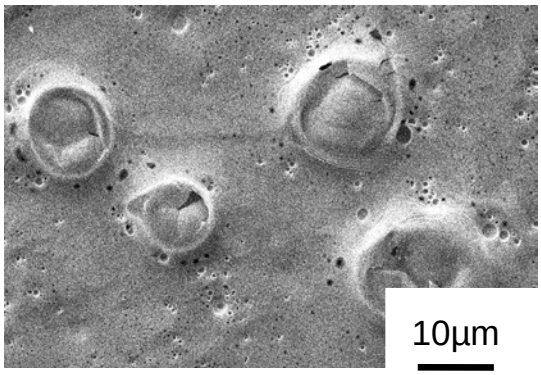

Fig. 1. SEM image taken from in boundary between melted and unmelted zone of the surface irradiated by an electron beam with a heat flux of 1 GW/m^2 and a duration of 1 ms. Sample is irradiated with 3.3 x 10^{23} He/m^2 at the peak temperature of 973 K before the electron bombardment.

採択課題番号 P8−13　高融点金属材料の高温下における応力負荷特性に及ぼす照射効果 プロジェクト（九大・応力研）徳永和俊、荒木邦明、藤原正、（九大・総理工）堀田智宏（京大・原子炉）徐　虬、義家敏正